scientific reports

Check for updates

OPEN

Aptamer-guided graphene oxide quantum dots for targeted suicide gene therapy in an organoid model of luminal breast cancer

Reza Taghizadeh-Tabarsi[1], Shiva Akbari-Birgani[1,2]✉, Mehrnaz Amjadi[1], Soheila Mohammadi[3], Nasser Nikfarjam[4,5] & Kosuke Kusamori[6]

Breast cancer is one of the most common cancers in women. One of the best therapeutic methods against breast cancer is gene therapy, while having an appropriate gene carrier is the biggest challenge of gene therapy. Hence, developing carriers with low cytotoxicity and high gene transfection efficiency, and preferentially with the selective function of gene delivery is a critical demand for this method. In the present study, we introduce a novel targeted carrier to deliver the inducible caspase-9 suicide gene (pLVSIN-iC9) into breast cancer cells. The carrier is composed of graphene oxide quantum dots decorated with polyethyleneimine, and S2.2; an aptamer with high affinity to MUC1 (GOQD-PEI/S2.2). Due to the overexpression of MUC1 in breast cancer cells, the designed GOQD-PEI/S2.2/pLVSIN-iC9 can selectively target cancer cells. Moreover, to better mimic solid tumor conditions, and to evaluate the selective effect of the GOQD-PEI/S2.2/pLVSIN-iC9, an organoid model derived from human dermal fibroblasts (HDF) and MCF-7 cells (coculture organoid) was generated and characterized. The results demonstrate that the coculture organoid model adapts the tissue structure of luminal breast cancer, as well. Therefore, the organoids were subjected to treatment with targeted gene therapy using GOQD-PEI/S2.2/pLVSIN-iC9. Our evidence supports the targeted killing effect of iC9 on the breast cancer cells of the organoids and suggests the good potential of the newly introduced carriers in targeted gene delivery.

Keywords Suicide gene therapy, Graphen oxide quantum dot (GOQD), Luminal breast cancer, Organoid model, Gene delivery

Abbreviations

GOQD	Graphene oxide quantum dots
PEI	Polyethylene imine
iC9	inducible Caspase 9
DLS	Dynamic light scattering
SEM	Scanning electron microscope

Cancer stands as the second leading global cause of mortality among diseases[1]. Among women, breast cancer prevails as the most frequent form of cancer. Tailoring treatment for breast cancer hinges on subtype, stage, and grade. Conventional breast cancer treatments encompass chemotherapy, radiotherapy, and endocrine therapy. Nonetheless, these approaches encounter challenges like treatment resistance. Consequently, it is crucial to identify treatment strategies with fewer impediments. One potential approach with reduced challenges is suicide gene therapy. inducible caspase 9 (iC9) is one of the suicide genes explored in breast cancer treatment is[2,3].

[1]Department of Biological Sciences, Institute for Advanced Studies in Basic Sciences (IASBS), Zanjan 4513766731, Iran. [2]Research Center for Basic Sciences and Modern Technologies (RBST), Institute for Advanced Studies in Basic Sciences (IASBS), Zanjan, Iran. [3]Pharmaceutical Sciences Research Center, Health Institute, Kermanshah University of Medical Sciences, Kermanshah, Iran. [4]Department of Chemical Engineering, College of Engineering and Computing, University of South Carolina, Columbia, SC 29208, USA. [5]Department of Chemistry, Institute for Advanced Studies in Basic Sciences (IASBS), Zanjan 4513766731, Iran. [6]Laboratory of Cellular Drug Discovery and Development, Faculty of Pharmaceutical Sciences, Tokyo University of Science, Chiba, Japan. ✉email: sh.akbari@iasbs.ac.ir

iC9 closely resembles caspase 9, a member of the caspase family, triggering apoptosis, albeit with a distinction: it features an FKBP12 domain rather than a CARD domain. Upon exposure to chemical inducers (such as AP1903), the two FKBP12 domains dimerize, triggering the dimerization of iC9. This dimerization process activates iC9, initiating apoptosis and culminating in cell death[2,4].

Selecting a suitable carrier stands as a prominent hurdle in gene therapy. Typically, gene carriers are divided into two primary categories: viral and non-viral carriers as like as Graphene oxide quantum dots (GOQD). GOQD, a zero-dimensional nanomaterial, feature hydroxyl, epoxy, and carboxyl functional groups. This nanomaterial boasts intriguing attributes such as an ultra-small size, high biocompatibility, and permeability through the plasma membrane. Thanks to its oxygenated functional groups and possible negative charges, GOQD disperses effectively in water, enhancing membrane permeability[5,6]. Conjugation of GOQD with positively charged substances such as Polyethyleneimine (PEI) converts it to a proper carrier for gene delivery[7]. Moreover, it can be decorated with some molecules with the aim of targeted therapy which potentially reducing the undesirable side effects and the necessary drug dosage[8,9].

Aptamers, short single-stranded DNA or RNA molecules, possess the ability to bind to specific target molecules. These molecules offer several advantages, including their small size, rapid tissue penetration, minimal toxicity, and cost-effective production[10]. MUC1, a glycoprotein, is typically found on the apical surface of most normal secretory epithelial cells. However, in breast cancer cells, a loss of cell polarity leads to a substantial up to 70% overexpression of MUC1. Various aptamers have been developed to target MUC1, and among them, the S2.2 aptamer stands out. Despite its higher cross-reactivity with albumin compared to the MA3 aptamer, the S2.2 aptamer boasts the lowest dissociation constant (Kd) and the highest affinity towards MUC1 among all introduced aptamers[11,12].

Two-dimensional (2D) models struggle to accurately replicate the intricate architecture of solid tumor structures. Additionally, these models fail to capture the multifaceted intricacies of the tumor microenvironment. Moreover, cells cultured in a 2D setup do not experience hypoxia conditions and exhibit distinct metabolic behaviors compared to actual solid tumors. As a result, a significant disparity emerges between the drug response observed in 2D cultures and that in real solid tumors[13]. Due to the convenience of 2D models, these models are very common. So that the evaluations on targeted drug delivery carriers are not only done on 2D models but also evaluate the effect of drug delivery carriers on targeting and non-targeting cells separately. The coculture of targeting and non-targeting cells in the 3D and organoid models can provide a more accurate and rigorous platform to evaluate the effectiveness of targeted drug delivery systems[14–16].

In this study, our objective was to develop a targetable carrier based on the PEI-decorated GOQD and S2.2, to facilitate the targeted transfection of the iC9 gene into the breast cancer cells. To be more accurate in evaluating the selective effect, in this study, for the first time, we use the coculture organoid model to evaluate the targeted gene delivery system. To the aim, the MCF-7-derived organoid models of breast cancer, including monoculture and coculture organoids were developed. Pathological studies on these models confirmed them as a luminal subtype of breast cancer. Comparative evaluation of these two models demonstrates the increased stemness state and cellular heterogeneity in coculture which makes it a better model for further studies by GOQD-PEI-S2.2/ pLVSIN-iC9.

Results

Characterization of GOQD-PEI/S2.2/pLVSIN-iC9 complex formation

A—Optimizing GOQD-PEI/S2.2/pLVSIN-iC9 complex formation through ratio Selection. To evaluate the binding of S2.2 to GOQD-PEI, a retardation assay with PAGE 16% was performed for the GOQD-PEI/S2.2/pLVSIN-iC9 with different ratios of its components. As shown in Fig. 1A, no band is seen for GOQD-PEI/S2.2/pLVSIN-iC9 with different ratios of GOQD-PEI to S2.2 in the PAGE, and only the band of the negative control containing S2.2 is seen. To evaluate the binding of pLVSIN-iC9 to the carrier, a retardation assay was performed. In none of the examined ratios of GOQD-PEI to S2.2, the band is not seen in the gel, and only the band of the negative control sample (pLVSIN-iC9) is seen (Fig. 1B). Since the GOQD-PEI/S2.2/ pLVSIN-iC9 is formed in all ratios, due to investigating the transfection rate in small amounts of the carrier and also preventing the cytotoxicity, the ratio of 0.03:2:1 (GOQD-PEI: S2.2: pLVSIN-iC9), which has the lowest amount of the carrier, was chosen for further investigations.

B—Confirmation of GOQD-PEI/S2.2/pLVSIN-iC9 Complex Formation. To confirm the generation of the GOQD-PEI/S2.2/pLVSIN-iC9, the absorption of the GOQD-PEI/S2.2/pLVSIN-iC9 components was measured separately and together over time. As shown in Fig. 1C, incubation of the GOQD-PEI/S2.2/pLVSIN-iC9 over time decreases the absorbance of the GOQD-PEI/S2.2/pLVSIN-iC9 at 260 nm wavelength. The absorbance of 260 nm confirms the formation of GOQD-PEI/S2.2.

Nano-Sized GOQD-PEI/S2.2/pLVSIN-iC9 complex

To evaluate the size of the generated GOQD-PEI/S2.2/pLVSIN-iC9 complex, DLS and SEM imaging were applied. DLS shows the average hydrodynamic size of 153 nm for the GOQD-PEI/S2.2/pLVSIN-iC9 (Fig. 2A). Also, the SEM image shows a round shape morphology for the GOQD-PEI/S2.2/pLVSIN-iC9 with a size ranging from 80 to 90 nm (Fig. 2B).

Cellular studies

The GOQD-PEI/S2.2/pLVSIN complex and its components are not cytotoxic

To measure the cytotoxicity of the generated GOQD-PEI/S2.2/pLVSIN-iC9 and its components, the GOQD-PEI/S2.2/pLVSIN-iC9 and its components were exposed to the MCF-7 cells for 72 h and then their viability was evaluated. As shown in Fig. 3A, no cytotoxicity is observed for the components of the GOQD-PEI/S2.2/pLVSIN-

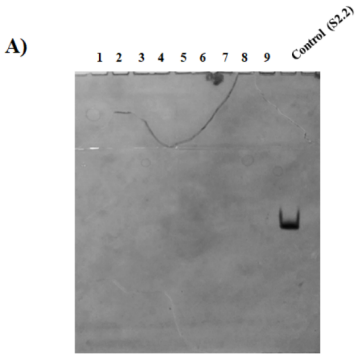

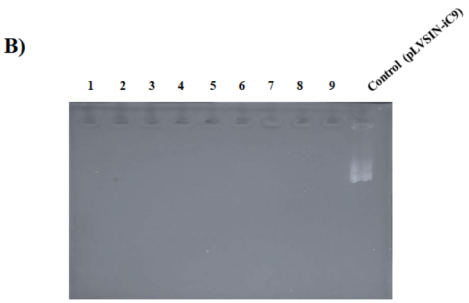

Ratio of components

Ratio	GOQD-PEI	S2.2	pLVSIN-iC9
0.03:10:1	5ng/µl	1500ng/µl	150ng/µl
0.8:17.1:1	133.3ng/µl	2571ng/µl	150ng/µl
1.1:2:1	170ng/µl	300ng/µl	150ng/µl
1.1:17.1:1	170ng/µl	2571ng/µl	150ng/µl
5:0.01:1	750ng/µl	2.57ng/µl	150ng/µl
5:10:1	750ng/µl	1500ng/µl	150ng/µl
5:20:1	750ng/µl	3000ng/µl	150ng/µl
8.8:2:1	1333ng/µl	300ng/µl	150ng/µl
10:10:1	1500ng/µl	1500ng/µl	150ng/µl

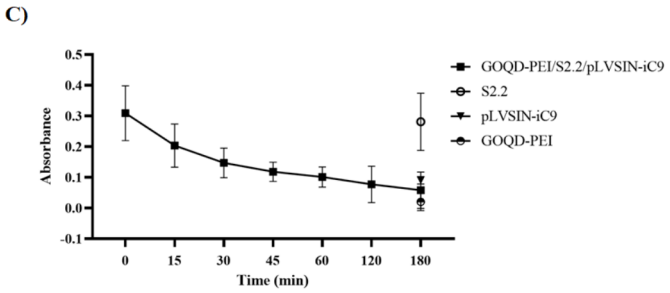

Fig. 1. The GOQD-PEI/S2.2/pLVSIN-iC9 is generated with different ratios of its components. Different ratios of components (1) 750ng/µl GOQD-PEI + 1500ng/µl S2.2 + 150ng/µl pLVSIN-iC9 (2) 133.3ng/µl GOQD-PEI + 2571ng/µl S2.2 + 150ng/µl pLVSIN-iC9 (3) 1500ng/µl GOQD-PEI + 1500ng/µl S2.2 + 150ng/µl pLVSIN-iC9 (4) 170ng/µl GOQD-PEI + 300ng/µl S2.2 + 150ng/µl pLVSIN-iC9 (5) 750ng/µl GOQD-PEI + 2.57ng/µl S2.2 + 150ng/µl pLVSIN-iC9 (6) 750ng/µl GOQD-PEI + 3000ng/µl S2.2 + 150ng/µl pLVSIN-iC9 (7) 170ng/µl GOQD-PEI + 2571ng/µl S2.2 + 150ng/µl pLVSIN-iC9 (8) 5ng/µl GOQD-PEI + 1500ng/µl S2.2 + 150ng/µl pLVSIN-iC9 (9) 1333ng/µl GOQD-PEI + 300ng/µl S2.2 + 150ng/µl pLVSIN-iC9 were mixed and incubated for 90 min. A gel retardation assay was performed. (**A**) polyacrylamide 16% gel electrophoresis. (**B**) Agarose 1% gel electrophoresis. (**C**) The generation of the GOQD-PEI/S2.2/pLVSIN-iC9 over time decreases the absorbance of the GOQD-PEI/S2.2/pLVSIN-iC9 at the wavelength of 260 nm.

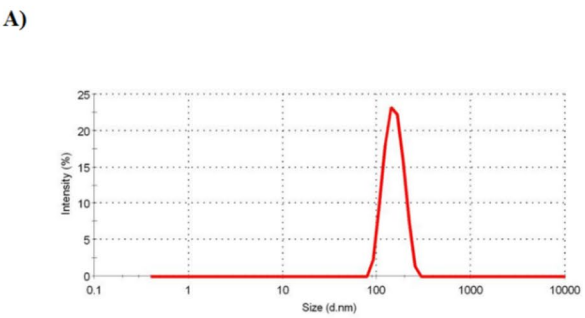

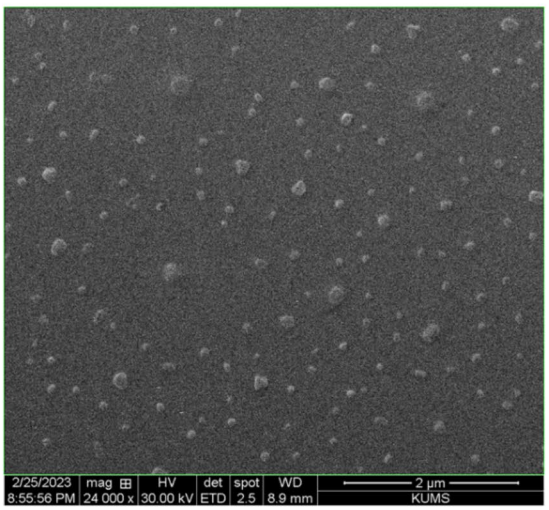

Fig. 2. The generated GOQD-PEI/S2.2/pLVSIN-iC9 has a nanometric size and spherical shape. (**A**) Size distribution of the GOQD-PEI/S2.2/pLVSIN-iC9 and calculated z-average hydrodynamic of around 153 nm. (**B**) SEM image shows the GOQD-PEI/S2.2/pLVSIN-iC9 size ranging from 80–90 nm.

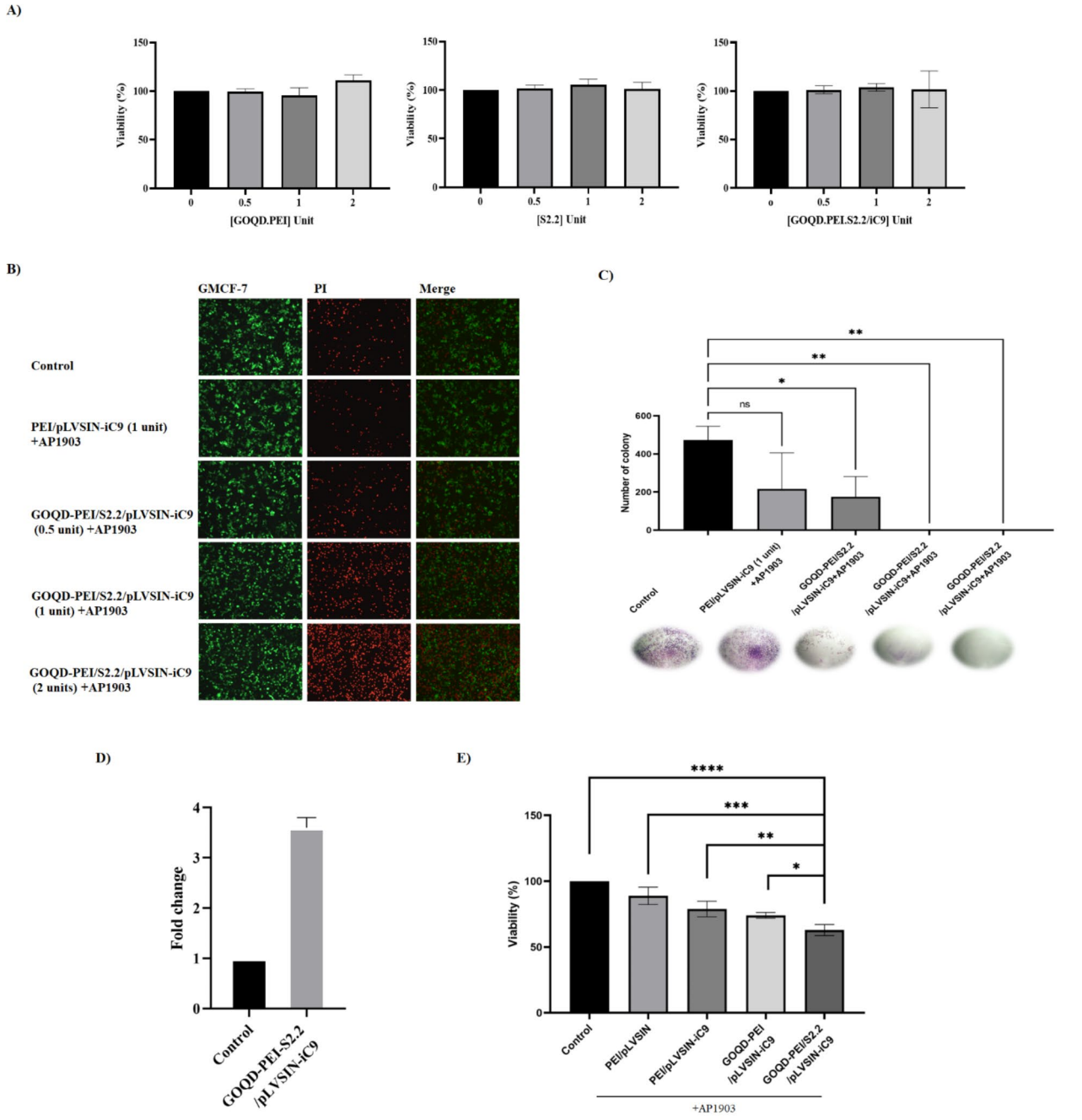

Fig. 3. The designed GOQD-PEI/S2.2/pLVSIN-iC9 causes cell death by high-efficiency iC9 gene transfection and inducible caspase-9 expression. (**A**) The GOQD-PEI/S2.2/pLVSIN-iC9 and its components were exposed to the MCF-7 cells for 72 h, and the viability of the cells was evaluated by the MTT method. The GOQD-PEI/S2.2/pLVSIN-iC9 and its components do not cause cytotoxicity (iC9 was not induced by AP1903). (**B**) The transfection effect was evaluated in the short term by fluorescent imaging. The PI color indicates cell death (Red), and green GMCF cells indicate live cells. Transfection of GOQD-PEI/S2.2/pLVSIN-iC9 after induction by AP1903, induces death well in the amount of 2 units. (**C**) Evaluating the effect of transfection in the long term with colony formation shows that the GOQD-PEI/S2.2/pLVSIN-iC9 in concentrations of 1 and 2 units effectively prevents the growth of cancer cells (induction by AP1903 was done, after transfection or all samples). (**D**) 48 h after transfection with the GOQD-PEI/S2.2/pLVSIN-iC9, the expression of the caspase9 gene was evaluated by RT-PCR. Transfecting the iC9 gene to the cells by the GOQD-PEI/S2.2/pLVSIN-iC9, increases the expression of caspase 9 compared to untreated cells. (**E**) pLVSIN-iC9 was transfected into the cells by GOQD-PEI/S2.2/pLVSIN-iC9, GOQD-PEI, and PEI, 48 h after transfection, cells were induced with AP1903 and 48 h after induction, cell viability was evaluated. Transfection of the iC9 gene by the generated GOQD-PEI/S2.2/pLVSIN-iC9 is more lethal than carriers such as GOQD-PEI and PEI (Each unit is defined as GOQD-PEI 5 ng, S2.2 300 ng and pLVSIN-iC9 150 ng).

iC9 and the complete GOQD-PEI/S2.2/pLVSIN-iC9 in different concentrations. It is noteworthy that iC9 was not induced by AP1903 (iC9 is dimerized and activated only by induction of AP1903).

Enhanced cell death and long-term inhibition of cancer cell growth achieved with GOQD-PEI/S2.2/pLVSIN-iC9 complex

To optimize the transfection rate and evaluate the transfection effect of the GOQD-PEI/S2.2/pLVSIN-iC9, iC9 functionality based on induction of cell death was evaluated. To do this, PI staining of GFP-expressing cells was performed. As shown in Fig. 3B, samples treated with 2 units of the GOQD-PEI/S2.2/pLVSIN-iC9 (Each unit is defined as GOQD-PEI 5 ng, S2.2 300 ng and pLVSIN-iC9 150 ng) by induction of AP1903, show a higher number of dead cells which are seen in red. To find the long-term effect of transfection using GOQD-PEI/S2.2, colony formation was done. The results of colony formation in Fig. 3C show that the transfection with 1 and 2 units of the GOQD-PEI/S2.2/pLVSIN-iC9 (by AP1903 induction) similarly prevents the growth of cancer cells. Since the administration of 2 units in both short- and long-term study studies showed a more significant effect, we chose it for further studies.

Transfection of the generated GOQD-PEI/S2.2/pLVSIN-iC9 increases the expression of caspase 9

To detect the expression of caspase-9 in MCF-7 cells, 48 h after the transfection of the iC9 with GOQD-PEI/S2.2/pLVSIN-iC9, the expression of caspase 9 was evaluated by Real-time PCR. As shown in Fig. 3D, transfection by the GOQD-PEI/S2.2/pLVSIN-iC9 caused a 3-fold increase in caspase 9 expression in transfected cells.

Comparative evaluation of transfection using GOQD-PEI/S2.2

To investigate the effect of the GOQD-PEI/S2.2/pLVSIN-iC9 on the transfection rate and compare it with other carriers, transfection was performed with PEI, GOQD-PEI and 2 units of GOQD-PEI/S2.2. 48 h after transfection, the cells were treated with AP1903, and their viability 48 h after induction was evaluated. As shown in Fig. 3E, cell viability in the group transfected with the generated GOQD-PEI/S2.2/pLVSIN-iC9 is significantly lower than transfection with other carriers. Which indicates its higher effectiveness in transfection.

Organoid models mimic the luminal breast cancer

The organoid models show the acini structures

To examine the growth kinetics of the organoids in both type of MCF-7 derived organoid (Mono culture organoid) and MCF-7 & HDF derived organoid (Coculture organoid), the size of organoids was measured in a 14-day time course. As it is apparent in Fig. 4A, from day 3 up to 8, the organoids are in growth phase and day 5 was selected for further studies. To evaluate the tissue structure of organoids, H&E staining was performed. Cells with different morphology were obvious, as well as acini structures (Fig. 4B). An interesting point is the smaller number of acini structures in coculture organoids compared to the monoculture one which might be due to the presence of fibroblasts in these organoids.

Expression of four main markers in organoids indicating the luminal subtype

Pathological subtyping of breast cancer relies on the presence or absence of specific proteins, including; ER (Estrogen Receptor), PR (Progesterone Receptor), HER2 (Human Epidermal Growth Factor Receptor 2), and Ki67. Accordingly, the expression profile of these markers in the generated organoids was evaluated by IHC staining. As shown in Fig. 4C, both monoculture and coculture organoids express ER and PR well, they don't express HER2 marker. Organoid models in both types have low expression of Ki67, it is to be noted that Ki67 expression increased in coculture organoids compared to monoculture organoids.

Fibroblasts increase the cellular heterogeneity of the organoids

To investigate tissue heterogeneity in organoid models and to evaluate the possible effect of the presence of fibroblasts, AE1/AE3, an epithelial marker, P63, myoepithelial marker, and vimentin, a mesenchymal marker, were investigated. As shown in Fig. 5A, mono-culture organoids express AE1/AE3 but they do not express P63 and vimentin, while coculture organoids express AE1/AE3, P63 and vimentin.

The presence of fibroblasts increases the stemness state of the organoids

To investigate the effect of fibroblast on the stemness state in organoid models, CD24 and CD44, the two known markers of breast cancer stem cells, were investigated[17]. As shown in Fig. 5B, the CD44-expressing cells are not observed in monoculture organoids, while the expression of the CD44 marker increases in coculture organoids.

GOQD-PEI/S2.2 targets MCF-7 cells in the coculture organoid model

To evaluate the effect of the generated GOQD-PEI/S2.2/pLVSIN-iC9 on the cell viability in the coculture organoid model, after GOQD-PEI/S2.2/pLVSIN-iC9 transfection and its induction, cell viability was evaluated. As shown in Fig. 6A, the transfection of the GOQD-PEI/S2.2/pLVSIN-iC9 and GOQD-PEI/pLVSIN-iC9 (GOQD-PEI/pLVSIN-iC9) decrease the cell viability of the coculture organoid models up to 80% and 60% respectively, but it does not affect the size of the coculture organoid models (data not shown). Coculture organoid models treated with GOQD-PEI/S2.2/pIRES2-GFP (nonrelevant DNA) do not show any cell death.

GOQD-PEI/S2.2/pLVSIN-iC9 removes MUC1 positive cells in the coculture organoid model

To investigate the effect of targeted gene delivery of the generated GOQD-PEI/S2.2/pLVSIN-iC9, pLVSIN-iC9 was replaced with FAM-labeled oligonucleotide in the GOQD-PEI/S2.2/pLVSIN-iC9 and it was used as a fluorescent GOQD-PEI/S2.2/pLVSIN-iC9 to identify MUC1(green), and the nuclei of cells were stained with PI

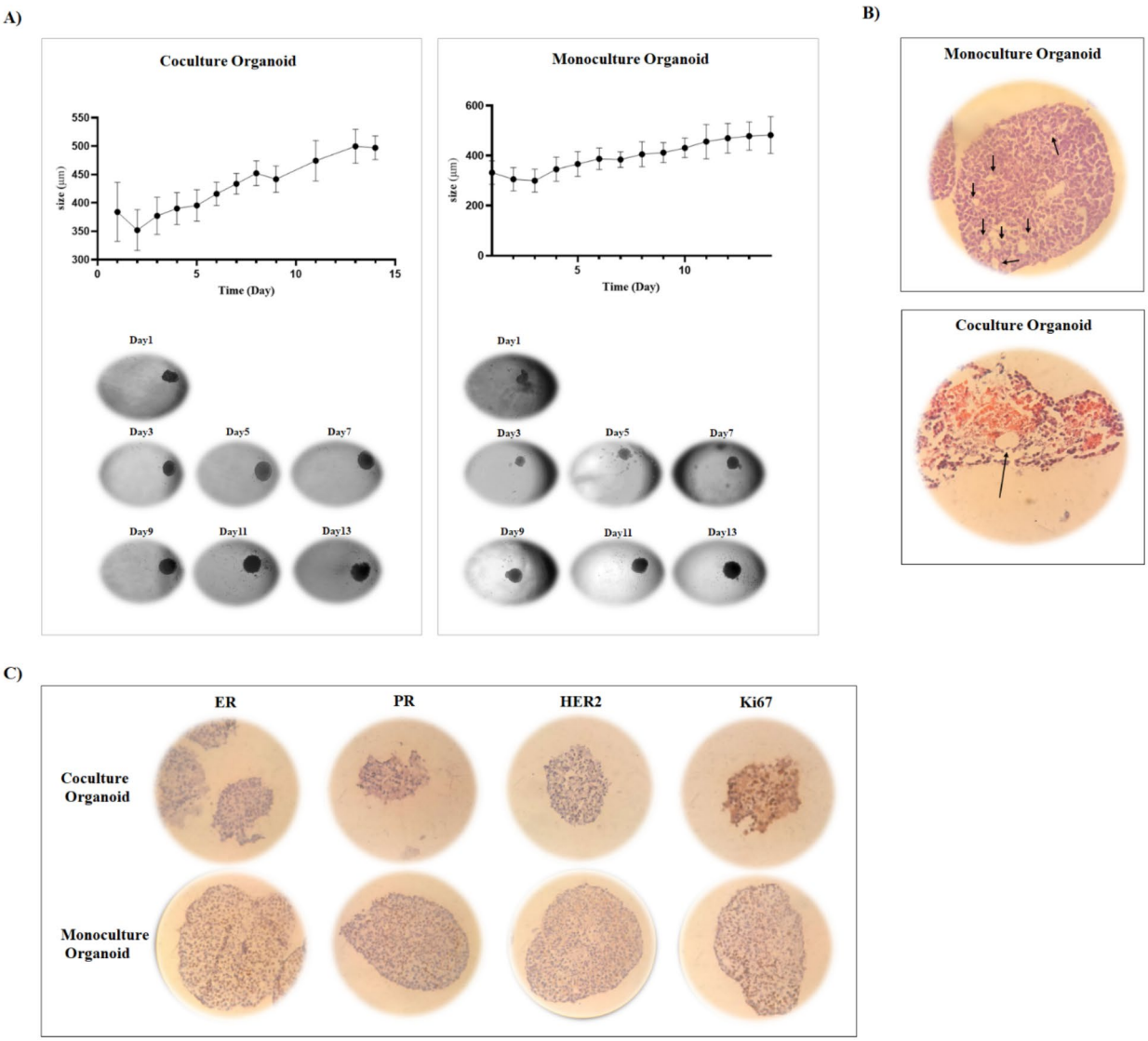

Fig. 4. The constructed organoid models mimic the characteristics of luminal tumors. (**A**) To check the organoid models' growth process, photographs were taken every day of the organoid models and their diameter was evaluated (4X magnification). organoid models are in the growth phase from the 3rd to the 8th day. (**B**) Hematoxylin-Eosin staining shows acinus structures in organoid models, the number of acini structures in coculture organoids is less than in monoculture organoids (40X magnification). (**C**) The expression of ER, PR, HER2 and Ki67 markers was evaluated by the IHC test. Organoid models, such as luminal tumors, express ER and PR well (40X magnification).

(red). As shown in Fig. 6B, the intensity of the yellow color as an indicator of MUC1-expressing cells is reduced in the coculture organoid models transfected with the GOQD-PEI/S2.2/pLVSIN-iC9.

Cells with MUC1 overexpression are targeted by the generated GOQD-PEI/S2.2/pLVSIN-iC9

To evaluate the targeting effect of the generated GOQD-PEI/S2.2/pLVSIN-iC9 on the coculture organoid model, transfection of the 5-day coculture organoid was done, and 48 h after transfection, induction with AP1903 was performed, and 48 h after induction, IHC test against MUC1 was performed. As shown in Fig. 6C, the cells that overexpressed MUC1 were removed in the transfected samples, and the total expression of MUC1 was reduced in the coculture organoid model.

Discussion

One of the critical elements in gene therapy is the choice of a convenient carrier. Ideally, these carriers should exhibit no or minimal cytotoxicity while demonstrating optimal transfection efficiency, ensuring effective gene delivery to the target cell or tissue[18,19]. A significant challenge in the realm of anticancer drugs lies in their

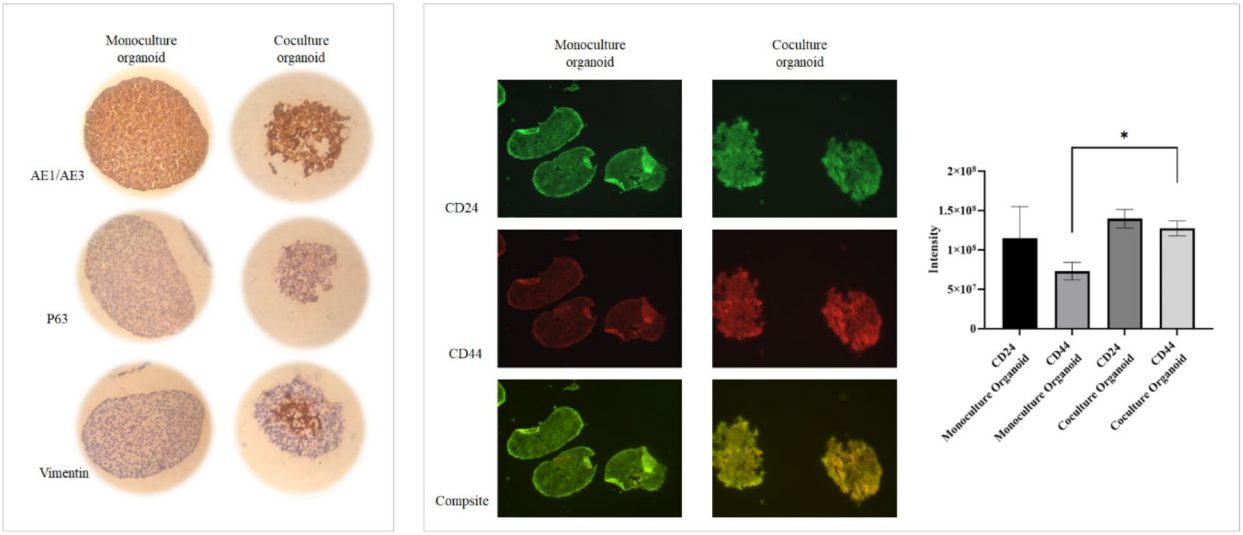

Fig. 5. Fibroblast increases heterogeneity and stemness state. Monoculture and coculture organoids were generated, and after 5 days organoids were blocked, and 5-micron sections were prepared. (**A**) Organoids with the presence of fibroblasts (coculture organoids) express AE1/AE3, P63 and Vimentin markers, but monoculture organoids only express AE1/AE3 marker (Magnification 40X). (**B**) The presence of fibroblast increases the expression of CD44 and increases the ratio of CD44 to CD24 expression, green color shows CD24 expression and red color shows CD44 expression (Magnification 20X).

potential adverse effects on healthy cells and tissues. The success of gene therapy for cancer hinges on precisely targeting and eliminating cancerous cells while sparing normal ones[8,19]. Recently, a nanoparticle was developed by grafting PEI onto GOQD, providing a safe and efficient carrier option with a favorable transfection rate[7]. In the present study, we attempt to advance it for targeting MUC1 positive cancer cells and evaluate its selective function in an organoid platform.

Primarily, the GOQD-PEI/S2.2/pLVSIN-iC9 complexes at different ratios were constructed and then the retardation assays were conducted. The outcomes revealed no observable free bands indicating the free pLVSIN-iC9 or free S2.2 which confirms that all components were successfully bound to GOQD-PEI in the ratios employed. A complex at 0.03:2:1 ratio of GOQD-PEI: S2.2: pLVSIN-iC9 with minimal GOQD-PEI content (5 ng/µl) was selected for evaluation of the absorbance changes over time. The decrease in absorbance provided further confirmation of GOQD-PEI/S2.2/pLVSIN-iC9 formation (Fig. 1). Although in other studies it has been shown that the DNA-Carrier complex usually forms in less than 15 min and its absorbance decreases[20–22], this study has shown that the decrease of the absorbance of the GOQD-PEI/S2.2/pLVSIN-iC9 takes about 90 min which can be due to a very small amount of GOQD-PEI, of course, investigating the precise reason requires further studies. Also, the reduction of the surface charge of GOQD-PEI due to the binding of pLVSIN-iC9 and S2.2 is a confirmation of the formation of the GOQD-PEI/S2.2/pLVSIN-iC9. In addition, the constancy of GOQD-PEI/S2.2/pLVSIN-iC9 absorbance at 260 nm wavelength shows that GOQD-PEI/S2.2/pLVSIN-iC9 is stable up to 14 days (Figure S1).

To obtain a comprehensive understanding of the size and morphology of the nanoparticles, SEM and DLS analysis were employed. The DLS showed particles with 153 nm while SEM images revealed 85 nm round particles (Fig. 2). However, it is important to note that SEM images displayed a limited number of aggregates with larger sizes, which accounts for the variance in size measurements obtained from these two methods. The presence of these larger particles has the effect of increasing the size measured by DLS due to heightened light scattering[23]. Consequently, DLS tends to report a larger size than the actual size of the particles[23,24].

Cytotoxicity assessments on the GOQD-PEI/S2.2 show that the GOQD-PEI/S2.2/pLVSIN, along with its individual components, did not exhibit any cytotoxic effects at the applied concentrations. To determine the optimal GOQD-PEI/S2.2 dosage for inducing cell death, short and long-term evaluations were performed, and results reveal that the 2-unit concentration is a good choice for the next studies. Real-time PCR confirmed the increased expression of caspase-9 in transfected cells. Furthermore, we compared the transfection efficiency of equal amounts of pLVSIN-iC9 using the GOQD-PEI/S2.2 and PEI, as a common transfection carrier. The results revealed that transfection with the GOQD-PEI/S2.2/pLVSIN-iC9 was significantly superior to PEI, effectively inhibiting the growth of the cancer cells. Considering the point that PEI has cytotoxicity by itself, these findings underscore the potency and superiority of the GOQD-PEI/S2.2/pLVSIN-iC9 as a transfection carrier in terms of both cytotoxicity and efficacy in inducing cell death. To assess the transfection rate of the nanoparticles, the function of GOQD-PEI/S2.2/pLVSIN-iC9, GOQD-PEI/pLVSIN-iC9 and PEI was studied using a death induction assay. The GOQD-PEI/S2.2/pLVSIN-iC9 induced significantly more cell death compared to the

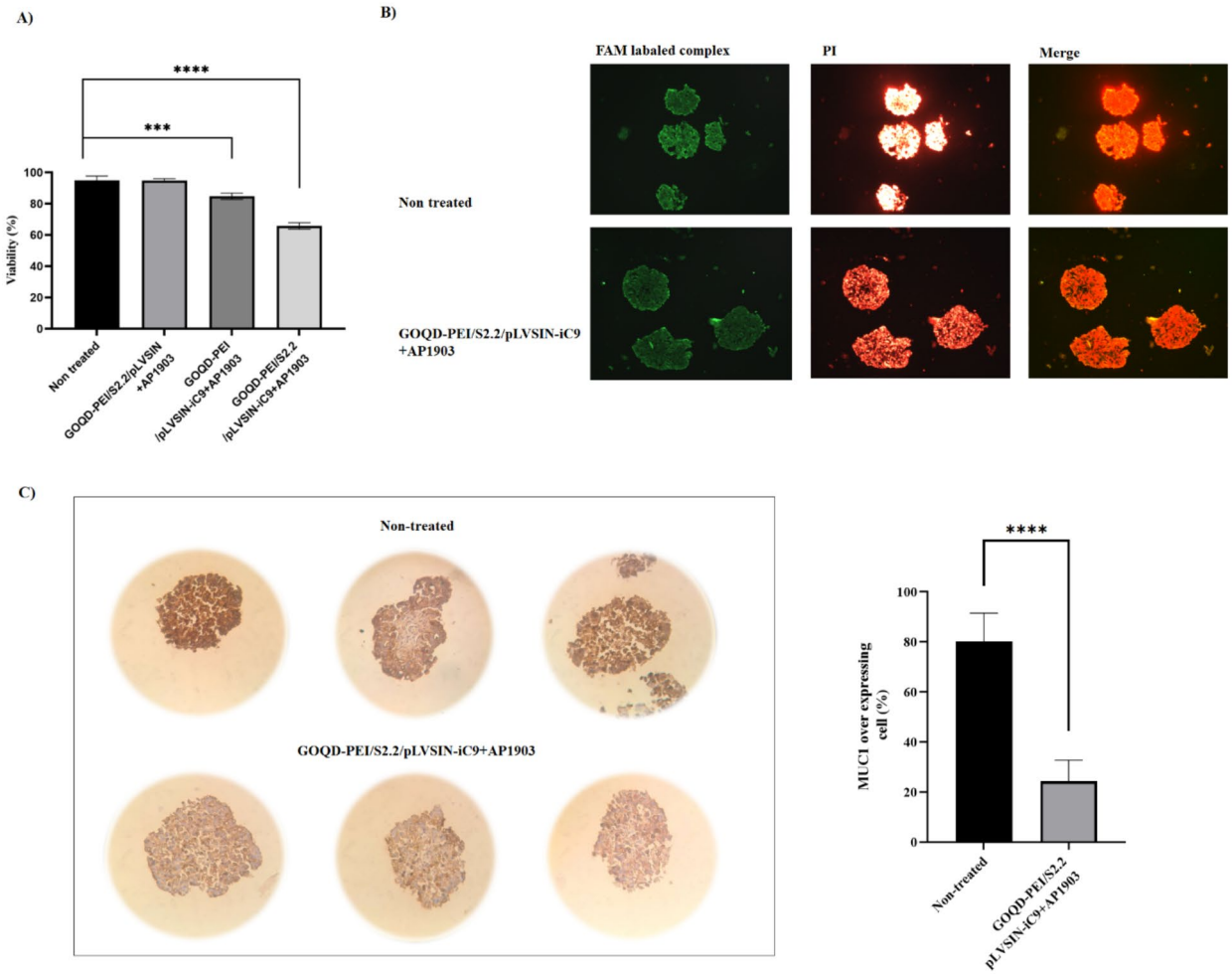

Fig. 6. The designed GOQD-PEI/S2.2/pLVSIN-iC9 targeting kills MUC1 overexpressing cells. (**A**) coculture organoid models were transfected by GOQD-PEI/S2.2/pLVSIN-iC9 and GOQD-PEI and induced with AP1903. 48 h after induction, cell viability was evaluated. Transfection by the GOQD-PEI/S2.2/pLVSIN-iC9 significantly reduces cell viability in the coculture organoid models. (**B**) FAM labeled oligonucleotide was bound to the GOQD-PEI/S2.2/pLVSIN-iC9 without pLVSIN-iC9 (green). This color GOQD-PEI/S2.2/pLVSIN-iC9 can determine MUC1-expressing cells. Transfected and non-treated coculture organoid models were incubated with colored GOQD-PEI/S2.2/pLVSIN-iC9 and nuclei were also stained with PI dye (red). The decrease of MUC1-expressing cells is seen in the coculture organoid models transfected with the GOQD-PEI/S2.2/pLVSIN-iC9 (Magnification 20X). (**C**) MUC1 expression in coculture organoid models untreated and transfected with GOQD-PEI/S2.2/pLVSIN-iC9 were investigated by IHC test. Transfection with the designed GOQD-PEI/S2.2/pLVSIN-iC9 reduces cells with MUC1 overexpression (Magnification 40X) The results were quantified by counting cells in 10 sections of coculture organoid.

GOQD-PEI/pLVSIN-iC9 and PEI. The enhanced cell death can be attributed to the GOQD-PEI/S2.2/pLVSIN-iC9 superior transfection rate, with the presence of S2.2 further augmenting this rate. In addition, as shown in Figure S2A, GOQD-PEI/S2.2 increases the transfection rate compared to lipofectamine as one of the common transfection carriers. The observed increase in transfection rate with the GOQD-PEI/S2.2/pLVSIN-iC9 may be due to a putative higher local concentration around MCF-7 cells. Notably, MCF-7 cells are known to overexpress MUC1 [25], and the GOQD-PEI/S2.2/pLVSIN-iC9 exhibits a strong affinity for MUC1, primarily due to the presence of S2.2. This heightened affinity for MUC1 likely contributes to the GOQD-PEI/S2.2/pLVSIN-iC9 superior transfection efficiency, ultimately resulting in increased cell death induction (Fig. 3). Although the presence of S2.2 increases the transfection rate of carrier to MCF-7 cells as target cells, the evaluation of the off-target effect shows that the presence of S2.2 does not increase the transfection rate to HDF cells as non-target cells, also, the affinity of the developed carrier in this study to transfect non-target cells is low (Figure S2).

To assess the selective functionality of the nanoparticles against breast cancer cells, it was imperative to choose an appropriate model. 2D models come with several limitations as they cannot accurately replicate the tumor structure, cellular interactions, cell polarity, and correct morphology found in actual tumors[26]. Therefore, to address these shortcomings and provide a more realistic context, organoid models have emerged that links in vitro studies to the human body, of course, it should be noted that in vivo models are beneficial

for investigating systemic effects, biodistribution and long-term safety. Herein, to evaluate the targeted drug delivery function of the developed carrier, we opted for a coculture organoid model. This choice aimed to bridge the gap and offer a comprehensive understanding of the complex human tumor microenvironment. The tumor microenvironment encompasses diverse cell types, including stromal cells, like fibroblasts which play pivotal roles. The interactions between stromal cells and cancer cells hold significant importance, as these interactions exert regulatory influences and can impact tumor growth, metastasis, and cancer progression[27,28]. Among stromal cells, fibroblasts occupy a unique and crucial position in this dynamic interplay.

Fibroblasts possess the capability to produce collagen effectively, allowing them to faithfully replicate the ECM characteristics found in breast cancer tumors. There are reports of increased drug resistance in organoid models compared to 2D culture models due to the increase of extracellular matrix (ECM) in organoid models[29]. Furthermore, the ECM in breast cancer tumors primarily consists of collagen. Notably, fibroblasts can contribute to drug resistance within spheroids, further complicating treatment strategies[30–33]. Research has shown that normal fibroblast cells can induce resistance to apoptosis in MCF-7 cells[34]. These findings emphasize the intricate interplay between fibroblasts, cancer cells, and the tumor microenvironment's significant impact on therapeutic responses.

Owing to the significant impact of fibroblasts, we consider them as a key stromal component in making the coculture organoids. Growth kinetic and tissue structure of the organoids were studied (Fig. 4). Mimicking tissue architecture is of paramount importance in this context, as alterations in tumor architecture can significantly influence cancer progression, and tissue architecture plays a crucial role in function. For instance, the acini structures in breast tissue, which are observable in the organoids, are a good indicator of the breast tissue[35,36]. with 2 unitsstructures are found in normal mammary tissue and low-grade mammary tumors, and as the grade of breast cancer and malignancy increases, acini structures decrease and disappear. Since fibroblast coculture with MCF-7 increases the production of MMPs and malignancy[37], it probably seems that in the coculture organoids, the number of the acini structures has been decreased, which mightily reflects the increase in malignancy of breast tumors[38–41]. Pathological analysis of the models exhibits characteristics indicative of being ER positive, PR positive, HER2 negative, and Ki67 low, resembling the luminal breast cancer. Moreover, the presence of fibroblasts in coculture organoids increases the expression of the Ki67 marker. The increase of the Ki67 marker is associated with the increase in malignancy[42]. An intriguing aspect to note is the complete molecular heterogeneity observed in the cells within the organoid models. This heterogeneity effectively mirrors the intra-tumor heterogeneity commonly seen in clinical breast cancer cases, adding further validity and relevance to the model for research purposes.

Tissue heterogeneity was assessed by examining the epithelial, myoepithelial, and mesenchymal markers (Fig. 5). Cells of the coculture organoids show high degree of heterogeneity. Interestingly, some cells showed P63 expression, while they were not seen in the initial cell population or even in the monoculture organoid. Therefore, it can be attributed to the presence of fibroblasts. Also, the expression of vimentin shows that fibroblasts are localized in the center of the coculture organoids. Moreover, in the presence of fibroblasts, the expression of CD44, the cancer stem cell marker associated with malignancy, has increased, too[43,44]. All together the data validates the coculture organoid as a proper model to investigate the selective function of the developed nanoparticle.

To study the impact of GOQD-PEI/S2.2/iC9 on the coculture organoid model, we came across a challenge with the colony formation assay due to the loss of MCF-7 cell attachment to the surface after coculture with HDF. This detachment phenomenon in MCF-7 cells cocultured with normal fibroblasts has been previously documented in other studies[45]. Consequently, we opted to examine the number of cells within the organoid and observed a significant increase in the ratio of dead cells to live cells in the group transfected with the GOQD-PEI/S2.2/iC9 (Fig. 6). These results suggest that the GOQD-PEI/S2.2/pLVSIN-iC9 may have a pronounced effect on cell viability within the coculture organoid. To examine the targeted gene delivery, the GOQD-PEI/S2.2 was labeled with FAM and dual staining was performed using the GOQD-PEI/S2.2/FAM (green) and PI (red). The PI-stained images showed that the coculture organoids transfected with the GOQD-PEI/S2.2/iC9 exhibited more black dots, indicating cell loss and empty spaces. Conversely, controls show a prevalence of red color, suggesting cell aggregations which were absent in the former group. These observations imply that the GOQD-PEI/S2.2/iC9 induces the evacuation of cell structures by removing certain cells within the coculture organoid. The yellow color in the merged images represents cells expressing MUC1. These yellow dots were prominent in the control group, but they are very few in the group treated with the GOQD-PEI/S2.2/pLVSIN-iC9. The shift from yellow to red in the treated group indicates the targeted removal of MUC1-expressing cells (yellow) and, notably, a majority of the remaining cells that do not express MUC1. These findings highlight the GOQD-PEI/S2.2/pLVSIN-iC9 potential for targeted gene delivery. To further confirm the observed targeting effects, MUC1 positive cells were studied by IHC. The results demonstrate that cells overexpressing MUC1 were effectively removed following transfection with the GOQD-PEI/S2.2/pLVSIN-iC9. Noteworthy, a previous study reports that epithelial secretory cells normally express MUC1, but in approximately 70% of breast cancer cases, cancer cells exhibit MUC1 overexpression[12]. Given this context, the developed GOQD-PEI/S2.2/pLVSIN-iC9 has good ability to target cells overexpressing MUC1 like breast cancer cells.

In this study, the selective ability of the GOQD-PEI/S2.2/pLVSIN-iC9 complex on the cocultures organoid model was investigated, while in other studies, the selective effect of targeted gene delivery complexes is often investigated separately on the 2D monoculture models of normal and cancer cells[14–16], which is of course valuable, but the coculture organoid models are more similar to solid tumors and provides a more realistic model for evaluating targeted gene delivery. Also, the selective effect of GOQD-PEI/S2.2/pLVSIN-iC9 complex was investigated on the organoid coculture model in which the increased expression of CD44 and Ki67 and the reduction of acini structures and the increase of heterogeneity were confirmed. Developed GOQD-PEI/S2.2/pLVSIN-iC9 with the ability of target breast cancer cells holds great promise for targeted gene delivery to breast

cancer cells, particularly those with a high transfection rate. This targeted approach has the potential to be an asset in breast cancer treatment and therapy development.

Materials and methods

GOQD-PEI synthesis

GOQD-PEI synthesis as described earlier by S. Mohammadi et al.[46]. briefly, GOQD was synthesized with citric acid and sodium hydroxide, then the carboxyl groups on the surface of GOQD was activated and PEI (25KD, Sigma) was covalently bonded by 1-ethyl-3-(3-dimethylaminopropyl) carbodiimide (EDC) and N-hydroxy succinimide (NHS).

Generation of GOQD-PEI/S2.2/pLVSIN-iC9 complex

To conjugate S2.2 and pLVSIN-iC9 to GOQD-PEI, various concentrations of GOQD-PEI; 5, 170, 750, 1333.3, 1500 (ng/µl) were incubated with HCl (1 N), then different concentrations of S2.2; 2.57, 300, 1500, 2571, 3000 (ng/µl) were added to each sample, and after pipetting, 150 ng/µl pLVSIN-iC9 was added to the samples. They were gently pipetted, and finally, GOQD-PEI/S2.2/pLVSIN-iC9 was incubated for 90 min at room temperature. Sequence of S2.2: 5′-TT CCC TT CC TTCT CT CTT CCT CT CTC CTT CTC TCT TCC TCT CTC CT TC*GCA GT TG AT CCT TGG ATAC CC TGG*-3′.

Gel retardation assay

Gel Retardation assay with agarose 1% and PAGE 16% were used to evaluate the binding of pLVSIN-iC9 to the GOQD-PEI and the binding of S2.2 to the GOQD-PEI, respectively. The GOQD-PEI/S2.2/pLVSIN-iC9 was prepared with ratios of (10:5:1, 17.1:8.8:1, 10:10:1, 2:1.1:1, 0.01:5:1, 20:5:1, 17.1:1.1:1, 10:0.03:1, 2:8.8:1). GOQD-PEI/S2.2/pLVSIN-iC9 with different ratios were mixed well with SYBR Green and loaded into the agarose 1%, and electrophoresis was performed for 40 min at 100 V. Also, the samples were loaded in PAGE 16% and after performing electrophoresis at 250 V for 150 min, they were stained with silver nitrate.

UV-Visible spectroscopy

To confirm the development of the GOQD-PEI/S2.2/pLVSIN-iC9, the absorption of the constituent components of the GOQD-PEI/S2.2/pLVSIN-iC9 separately and the generated GOQD-PEI/S2.2/pLVSIN-iC9 was measured by the spectrophotometer (Spectrum SP-UV 500DB/VDB). The absorption of GOQD-PEI (5 ng/µl), S2.2 (300 ng/µl), and pLVSIN-iC9 (150 ng/µl) were measured at 260 nm. After that, the GOQD-PEI/S2.2/pLVSIN-iC9 components were mixed gently and incubated. The absorbance of samples was measured at 260 nm in various time points of incubation; 0, 15, 30, 45, 60, 120, and 180 min.

Evaluation of the size of GOQD-PEI/S2.2/pLVSIN-iC9

To measure the size and shape of the generated GOQD-PEI/S2.2/pLVSIN-iC9, the GOQD-PEI/S2.2/pLVSIN-iC9 was prepared with ratios of 30:60:1, it was vacuum coated with a thin gold layer, then the sample was imaged with scanning electron microscopy (SEM) (FEI Quanta 450).

Cell culture and developing the organoid models

MCF-7 (BN_0012.1.7) and HDF (BN_0012.1.32) cells (Bon Yakhteh Company) were cultured in complete medium containing DMEM high glucose, 10% fetal bovine serum (FBS, Gibco), and 1% penicillin-streptomycin in 37 °C, 5% CO_2 and 95% humidity condition. When the cells were confluent, the cells were trypsinized and applied to generate the organoid model (Trypsin-EDTA, BIO-IDEA). A cell suspension was prepared with a 1:1 ratio of MCF-7 and HDF. A cell suspension containing 80,000 cells/ml was added to each well of an agarose-coated 96-well plate and incubated for up to 14 days (Agarose, Sigma). Imaging of the samples was done every day. The changes in size of organoids were evaluated by measuring the area of the organoids using Image J software and their growth curve in a 15-day time course was plotted.

Evaluation of the cytotoxicity of carrier and carrier with non-relevant plasmid

To investigate the cytotoxicity of the GOQD-PEI/S2.2/pLVSIN-iC9, MCF-7 cells were seeded in a 96-well plate (20000 cells/well). After 24 h, the cells were treated by GOQD-PEI, S2.2 and GOQD-PEI/S2.2/pLVSIN with concentrations of 0.5, 1 and 2 units, each unit is defined as GOQD-PEI (5 ng), S2.2(300 ng) and pLVSIN (150 ng) that added to 200 µl of culture medium on the cells then incubated for 72 h. After incubation the medium was replaced with MTT solution (0.5 mg/ml) and the cells were incubated for 4 h. After incubation, the MTT solution was drained and 100 µL of DMSO was added to each well and pipetted. The absorbance was measured at 490 nm with an ELISA reader (BioTek).

Evaluating the transfection rate of the developed GOQD-PEI/S2.2/pLVSIN-iC9

To evaluate the transfection rate in different concentrations of the GOQD-PEI/S2.2/pLVSIN-iC9 (0.5, 1 and 2 unit), 25,000 MCF-7 cells stably expressing GFP (GMCF-7) were seeded in each well of a 96-well plate. 24 h later, the cells starved with serum free media for 2 h. The cells were exposed to GOQD-PEI/S2.2/pLVSIN-iC9 for 6 h, after that the complete media was replaced. 48 h after transfection, iC9 was induced with AP1903 with concentration of 100 nM.

Propidium Iodide (PI) staining-for short-term evaluation PI staining was conducted. 24 h after induction by AP1903, cells were stained by PI with concentration of 1 µg/ml for 5 min and imaged with a fluorescent microscopy by green and red filters (Optika).

Colony formation assay-For long-term evaluation, a colony formation test was performed. 24 h after induction, the cells were singled using trypsin and re-seeded in a 24-well plate, and after 10 days, media was

removed, cells were washed using PBS and fixed with methanol and stained with crystal violet. The stained samples were observed using light microscopy (Nikon). The images were analyzed using ImageJ software.

Real-time PCR

To measure the expression of inducible caspase 9 in transfected cells, Real-time PCR was performed. 48 h after the transfection of MCF-7 cells with GOQD-PEI/S2.2/pLVSIN-iC9, the cells were singled using trypsin and RNAs were extracted using an RNA extraction kit (Bio basic). 200 ng of total RNAs was used to cDNA synthesis (Amplicon kit). To perform Real-time PCR, 50 ng of cDNA, master mix and forward and reverse primers with ATTCTCGAGACCATGGGAGTGCAGGTG and ATTGAATTCTTAGTCGAGTGCGTAGTCTGG sequences were used, respectively. The fold change was evaluated by the ΔΔCT method. β actin was used as an internal control for normalization.

Investigating the effect of S2.2 on transfection rate

To evaluate the effect of S2.2 on transfection rate and compare GOQD-PEI/S2.2/pLVSIN-iC9 with its component, 20,000 MCF-7 cells were seeded in each well of a 96-well plate, after 24 h, pLVSIN-iC9 transfection was performed with PEI, GOQD-PEI and GOQD-PEI/S2.2 as a carrier. 48 h after transfection, iC9 was induced with AP1903 (100 nM), and 48 h after induction, cell viability was evaluated by MTT test.

Evaluating the effect of the GOQD-PEI/S2.2/pLVSIN-iC9 on the coculture organoid model

To investigate the effect of the GOQD-PEI/S2.2/pLVSIN-iC9 on cell viability of coculture organoid models, 5 days after generation of the coculture organoid models, transfection was performed with GOQD-PEI/S2.2/pLVSIN, GOQD-PEI/pLVSIN-iC9 and GOQD-PEI/S2.2/pLVSIN-iC9, 48 h after transfection, coculture organoids were treated with AP1903, and 48 h after induction, coculture organoid model cells were singled and incubated with trypan blue dye (0.4% in PBS) for 4 min. After that, the number of stained cells (dead cells) and unstained cells (live cells) was counted with a light microscope (Cannon).

Immunohistochemistry

To investigate the effect of targeted drug delivery of the GOQD-PEI/S2.2/pLVSIN-iC9 on the coculture organoid model, the 5-day coculture organoid models were transfected with GOQD-PEI/S2.2/pLVSIN-iC9. 48 h after transfection, iC9 was induced with AP1903, and 48 h after induction, treated and untreated coculture organoid models were embedded in paraffin and 5-micron sections were taken. The sections were deparaffinized and rehydrated on a charged slide, then blocked, and incubated with Mouse anti-human Mucin 1 Monoclonal Antibody clone ZM35 and detection was done with the master polymer plus detection system (HRP) with DAB and samples were counterstained with hematoxylin. The stained samples were observed using light microscopy (Nikon).

Statistical analysis

Statistical analyses were performed using Graph pad Prism 9 software and the one-way ANOVA method was used to evaluate the significance of differences. In this study, P value ≤ 0.05 was considered significant. All tests were done at least in triplicates.

Data availability

Data is provided within the manuscript or supplementary information files.

Received: 18 March 2024; Accepted: 25 September 2024
Published online: 15 October 2024

References

1. Woollam, M. et al. Urinary volatile terpenes analyzed by gas chromatography–mass spectrometry to monitor breast cancer treatment efficacy in mice. *J. Proteome Res.* **19**, 1913–1922 (2020).
2. Mohseni-Dargah, M., Akbari-Birgani, S., Madadi, Z., Saghatchi, F. & Kaboudin, B. Carbon nanotube-delivered iC9 suicide gene therapy for killing breast cancer cells in vitro. *Nanomedicine* **14**, 1033–1047 (2019).
3. Moradi-Mehr, S. et al. Comparative evaluation of the therapeutic strategies using a minimal model of luminal breast cancer. *Biochem. Biophys. Res. Commun.* **666**, 107–114 (2023).
4. Li, P. et al. Caspase-9: Structure, mechanisms and clinical application. *Oncotarget* **8**, 23996 (2017).
5. Ahirwar, S., Mallick, S. & Bahadur, D. Electrochemical method to prepare graphene quantum dots and graphene oxide quantum dots. *ACS Omega* **2**, 8343–8353 (2017).
6. Li, S. et al. Antibacterial thin film nanocomposite reverse osmosis membrane by doping silver phosphate loaded graphene oxide quantum dots in polyamide layer. *Desalination* **464**, 94–104 (2019).
7. Mohammadi, S., Akbari-Birgani, S., Nikfarjam, N. & Rasekhian, M. Polyethyleneimine-decorated graphene oxide quantum dot as a carrier for suicide gene delivery to the breast three-dimensional cancer model. *J. Drug Deliv. Sci. Technol.*, 104849 (2023).
8. Kumari, P., Ghosh, B. & Biswas, S. Nanocarriers for cancer-targeted drug delivery. *J. Drug Target.* **24**, 179–191 (2016).
9. Liyanage, P. Y. *et al.* Nanoparticle-mediated targeted drug delivery for breast cancer treatment. *Biochimica et Biophysica Acta (BBA)-Reviews on Cancer* **1871**, 419–433 (2019).
10. Yazdian-Robati, R. et al. Smart aptamer-modified calcium carbonate nanoparticles for controlled release and targeted delivery of epirubicin and melittin into cancer cells in vitro and in vivo. *Drug Dev. Ind. Pharm.* **45**, 603–610 (2019).
11. Ferreira, C., Matthews, C. & Missailidis, S. DNA aptamers that bind to MUC1 tumour marker: Design and characterization of MUC1-binding single-stranded DNA aptamers. *Tumor Biol.* **27**, 289–301 (2006).
12. Nabavinia, M. S. et al. Anti-MUC1 aptamer: A potential opportunity for cancer treatment. *Med. Res. Rev.* **37**, 1518–1539 (2017).
13. Huang, B.-W. & Gao, J.-Q. Application of 3D cultured multicellular spheroid tumor models in tumor-targeted drug delivery system research. *J. Controlled Release* **270**, 246–259 (2018).

14. Meng, L. et al. Aptamer-guided DNA tetrahedrons as a photo-responsive drug delivery system for Mucin 1-expressing breast cancer cells. *Appl. Mater. Today* **23**, 101010 (2021).
15. Shahrad, S., Rajabi, M., Javadi, H., Karimi Zarchi, A. A. & Darvishi, M. H. Targeting lung cancer cells with MUC1 aptamer-functionalized PLA-PEG nanocarriers. *Sci. Rep.* **12**, 4718 (2022).
16. Zolbanin, N. M. et al. Targeted co-delivery of docetaxel and cMET siRNA for treatment of mucin1 overexpressing breast cancer cells. *Adv. Pharm. Bull.* **8**, 383 (2018).
17. Ricardo, S. et al. Breast cancer stem cell markers CD44, CD24 and ALDH1: Expression distribution within intrinsic molecular subtype. *J. Clin. Pathol.* **64**, 937–946 (2011).
18. Goverdhana, S. et al. Regulatable gene expression systems for gene therapy applications: Progress and future challenges. *Molecular Therapy* **12**, 189–211 (2005).
19. Scanlon, K. J. Cancer gene therapy: Challenges and opportunities. *Anticancer Res.* **24**, 501–504 (2004).
20. Zuidam, N. J. & Barenholz, Y. Electrostatic and structural properties of complexes involving plasmid DNA and cationic lipids commonly used for gene delivery. *Biochimica et Biophysica Acta (BBA)-Biomembranes* **1368**, 115–128 (1998).
21. Erbacher, P. et al. Genuine DNA/polyethylenimine (PEI) complexes improve transfection properties and cell survival. *J. Drug Target.* **12**, 223–236 (2004).
22. Kaboudin, B., Saghatchi, F., Kazemi, F. & Akbari-Birgani, S. A novel magnetic carbon nanotubes functionalized with pyridine groups: Synthesis, characterization and their application as an efficient carrier for plasmid DNA and aptamer. *ChemistrySelect* **3**, 6743–6749 (2018).
23. Souza, T. G., Ciminelli, V. S. & Mohallem, N. D. S. in *J. Phys. Conf. Ser.* 012039 (IOP Publishing).
24. Panchal, J., Kotarek, J., Marszal, E. & Topp, E. M. Analyzing subvisible particles in protein drug products: A comparison of dynamic light scattering (DLS) and resonant mass measurement (RMM). *AAPS J.* **16**, 440–451 (2014).
25. Yu, C. et al. Novel aptamer-nanoparticle bioconjugates enhances delivery of anticancer drug to MUC1-positive cancer cells in vitro. *PLoS ONE* **6**, e24077 (2011).
26. Kapałczyńska, M. et al. 2D and 3D cell cultures—A comparison of different types of cancer cell cultures. *Arch. Med. Sci.* **14**, 910–919 (2018).
27. Lazzari, G., Couvreur, P. & Mura, S. Multicellular tumor spheroids: A relevant 3D model for the in vitro preclinical investigation of polymer nanomedicines. *Polym. Chem.* **8**, 4947–4969 (2017).
28. Bourhis, X. D. L. et al. Effect of stromal and epithelial cells derived from normal and tumorous breast tissue on the proliferation of human breast cancer cell lines in co-culture. *Int. J. Cancer* **71**, 42–48 (1997).
29. Karimifard, S. A., Salehzadeh-Yazdi, A., Taghizadeh-Tabarsi, R. & Akbari-Birgani, S. Mechanical effects modulate drug resistance in MCF-7-derived organoids: Insights into the wnt/β-catenin pathway. *Biochem. Biophys. Res. Commun.*, 149420 (2023).
30. Stock, K. et al. Capturing tumor complexity in vitro: Comparative analysis of 2D and 3D tumor models for drug discovery. *Sci. Rep.* **6**, 28951 (2016).
31. Xin, X. & Yang, S.-T. A dual fluorescent 3-D multicellular coculture of breast cancer MCF-7 and fibroblast NIH-3T3 cells for high throughput cancer drug screening. *Biochem. Eng. J.* **148**, 152–161 (2019).
32. Krause, S., Maffini, M. V., Soto, A. M. & Sonnenschein, C. The microenvironment determines the breast cancer cells' phenotype: Organization of MCF7 cells in 3D cultures. *BMC Cancer* **10**, 1–13 (2010).
33. Kim, S. H. et al. Role of secreted type I collagen derived from stromal cells in two breast cancer cell lines. *Oncol. Lett.* **8**, 507–512 (2014).
34. Morgan, M. M. et al. Mammary fibroblasts reduce apoptosis and speed estrogen-induced hyperplasia in an organotypic MCF7-derived duct model. *Sci. Rep.* **8**, 7139 (2018).
35. Murtagh, J. et al. Organization of mammary epithelial cells into 3D acinar structures requires glucocorticoid and JNK signaling. *J. Cell Biol.* **166**, 133–143 (2004).
36. Swamydas, M., Eddy, J. M., Burg, K. J. & Dréau, D. Matrix compositions and the development of breast acini and ducts in 3D cultures. *In Vitro Cell. Dev. Biol. Anim.* **46**, 673–684 (2010).
37. Ito, A., Nakajima, S., Sasaguri, Y., Nagase, H. & Mori, Y. Co-culture of human breast adenocarcinoma MCF-7 cells and human dermal fibroblasts enhances the production of matrix metalloproteinases 1, 2 and 3 in fibroblasts. *Brit. J. Cancer* **71**, 1039–1045 (1995).
38. Bissell, M. J. et al. Tissue structure, nuclear organization, and gene expression in normal and malignant breast. *Cancer Res.* **59**, 1757s–1764s (1999).
39. Weaver, V. M. et al. Reversion of the malignant phenotype of human breast cells in three-dimensional culture and in vivo by integrin blocking antibodies. *J. Cell Biol.* **137**, 231–245 (1997).
40. Pratap, J. et al. Ectopic runx2 expression in mammary epithelial cells disrupts formation of normal acini structure: Implications for breast cancer progression. *Cancer Res.* **69**, 6807–6814 (2009).
41. Fournier, M. V. et al. Gene expression signature in organized and growth-arrested mammary acini predicts good outcome in breast cancer. *Cancer Res.* **66**, 7095–7102 (2006).
42. Wintzer, H. O., Zipfel, I., Schulte-Mönting, J., Hellerich, U. & von Kleist, S. Ki-67 immunostaining in human breast tumors and its relationship to prognosis. *Cancer* **67**, 421–428 (1991).
43. Ji, P. et al. CD44hiCD24lo mammosphere-forming cells from primary breast cancer display resistance to multiple chemotherapeutic drugs. *Oncol. Rep.* **35**, 3293–3302 (2016).
44. Van Phuc, P. *et al.* Downregulation of CD44 reduces doxorubicin resistance of CD44+ CD24− breast cancer cells. *OncoTargets Therapy*, 71–78 (2011).
45. Adam, L., Crepin, M., Lelong, J. C., Spanakis, E. & Israel, L. Selective interactions between mammary epithelial cells and fibroblasts in co-culture. *Int. J. Cancer* **59**, 262–268 (1994).
46. Mohammadi, S., Akbari-Birgani, S., Nikfarjam, N. & Rasekhian, M. Polyethyleneimine-decorated graphene oxide quantum dot as a carrier for suicide gene delivery to the breast cancer three-dimensional model. *J. Drug Deliv. Sci. Technol.* **88**, 104849 (2023).

Author contributions

The research was supervised by S.A.B. The experiments were conducted by R.T.T., M.A. and S.M. Plasmid was provided by K.K. The analysis and interpretation of the data were done by S.A.B., R.T.T, M.A., S.M., N.N. The paper was written by S.A.B., and R.T.T, and reviewed by all the authors.

Funding

This work was supported by financial support from the Iran National Science Foundation (INSF) [grant number 4026873] and the Institute for Advanced Studies in Basic Sciences (IASBS) (grant number G2022IASBS32635).

Declarations

Competing interests
The authors declare no competing interests.

Additional information
Supplementary Information The online version contains supplementary material available at https://doi.org/10.1038/s41598-024-74312-9.

Correspondence and requests for materials should be addressed to S.A.-B.

Reprints and permissions information is available at www.nature.com/reprints.

Publisher's note Springer Nature remains neutral with regard to jurisdictional claims in published maps and institutional affiliations.